Presented at the
11th International Meeting of the
Society of Nuclear Medicine,
Athens, Greece,
September 24-29, 1973

LBL-2161

c.1

QUANTITATIVE SEQUENTIAL IMAGING OF RADIONUCLIDE DISTRIBUTION USING THE WHOLE-BODY SCANNER AND THE GAMMA CAMERA: ABSOLUTE ACCURACY AND ASPECTS OF THREE-DIMENSIONAL RECONSTRUCTION

T. F. Budinger, G. T. Gullberg, M. L. Nohr,
J. McRae and H. O. Anger

September 1973

Prepared for the U. S. Atomic Energy Commission
under Contract W-7405-ENG-48

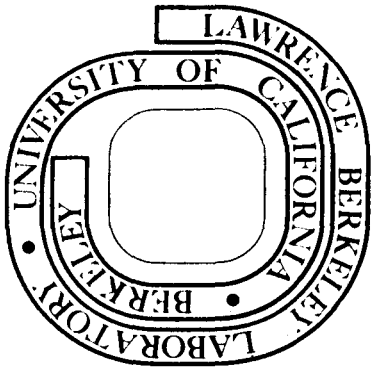

LBL-2161

DISCLAIMER

QUANTITATIVE SEQUENTIAL IMAGING OF RADIONUCLIDE DISTRIBUTION USING THE WHOLE-BODY SCANNER AND THE GAMMA CAMERA: Absolute accuracy and aspects of three-dimensional reconstruction.

T. F. Budinger, G. T. Gullberg, M. L. Nohr, J. McRae and H. O. Anger

Donner Laboratory and Lawrence Berkeley Laboratory
University of California, Berkeley

SCOPE

We report here the progress in quantitating the distribution of isotope within organs on sequential images of the whole body using the whole-body scanner, and on techniques of reconstructing the three-dimensional distribution from multiple gamma-camera views using a variety of different algorithms.

WHOLE-BODY SCAN QUANTITATION

The following variables are involved in the precise quantitation of the amount of radiopharmaceuticals in regions of the body: (1) geometry effect, (2) patient thickness, (3) thickness and homogeneity of isotope distribution, (4) source position, (5) photon attenuation coefficient. The whole-body scanner at Donner Laboratory consists of 64 detectors distributed as four rows of 16 detectors with a diagonal offset to give good resolution and adequate collimation between the single 3.2-cm diameter by 3.8-cm thick sodium iodide (Tl) crystals (Anger, 1966). The patient is positioned on a bed that is moved over the detector array and pulse-height selection is used to separate pulses between different isotopes. The scan durations can vary from 0.75 minute to hours.

The table position, detector identification, and isotope are encoded by a hardware device that presents the computer with a 16-bit word. A 2048-word buffer is filled every 8 of 384 table positions with data from up to 4 isotopes. As this buffer is being filled, another buffer is dumped onto the raw data disc, and after the data accumulation these data are framed into 6 frames of 64 X 64, which takes less than 10 seconds (Budinger, 1973). A light pen is used to delineate up to 16 irregular areas of kidney, bone, heart, etc. for integration. A special detector sensitivity-correction program is applied to the data as they are being framed, and a routine for off-setting patient position is used for making sequential comparisons of the change in distribution of isotope. If the quantitation is done on an organ region basis rather than an element by element basis using both supine and prone scans (conjugate scanning), then the geometry effect and source position should be negligible for most situations. The slight geometry effect was found to be insignificant and has not been included in this analysis.

Isotope distribution and homogeneity as well as body thickness has been taken into account by a correction factor and the activity is calculated from

$$A = \frac{\sqrt{A_p \cdot A_s}\; e^{\mu T/2} f\mu T}{2\, c \sinh (f\mu T/2)} \qquad (1)$$

where A_p and A_s are the prone and supine scans, T is the thickness, μ

is the attenuation coefficient, and f is the fraction of T occupied by the isotope.

The importance of body thickness on the accuracy is reflected in the relationship of the change in the correction factor to the geometric mean $(A_p \cdot A_s)^{1/2}$ of eq(1) as body thickness increases. For a given thickness the change in this correction factor will change according to the fraction of body thickness, f, over which the isotope is considered to be distributed; however, this is shown to be of little importance (Fig. 1). An estimate of f = 2/3 has been shown by Sorenson (1971) to be adequate, and our analysis corroborates his work.

The contribution from attenuation through the body is not accurately given by a constant attenuation coefficient, μ; however, for photons above ~100 keV we do not expect this to lead to significant errors.

Representative results from calibration trials are shown in Table 1 for both ^{99m}Tc and ^{131}I. Sources of different concentration in different volumes attenuated by various thicknesses of scattering media were used with the whole-body scanner. The accuracy of quantitation is ±10% using the geometric mean arrived at by supine and prone scans when target to nontarget ratios are greater than 10:1. Background or cross-talk can be removed by subtracting assumed contributions using information of activity from tissues contiguous to the organ of interest.

PATIENT STUDIES

The organ by organ (e.g., brain, heart, liver, kidney, bone, soft tissue, etc.) distribution of the following radionuclides has been followed from days to months: ^{18}F, ^{24}Na, ^{37}Br, ^{43}K, ^{51}Cr, ^{52}Fe, ^{111}In, ^{75}Se-methionine, ^{99m}Tc-EHDP, ^{131}I-19-iodocholesterol, ^{81}Rb. An example of sequential studies extending 9 half-lives for ^{81}Rb is shown as Fig. 2, and the sequential distribution of ^{131}I-iodocholesterol over a period of 7 days is shown as Fig. 3. The quantitative regional-distribution for ^{131}I-iodocholesterol is described by Table 2 wherein the fraction of the injected dose for each important body region has been calculated These data show features of isotope redistribution that have not heretofore been noted, and will provide the basic biological data for more exact dosimetry.

FUTURE APPLICATIONS OF WHOLE-BODY SCANNER QUANTITATIVE-SYSTEM

In addition to the direct quantitation discussed above, the whole-body scanner provides a unique opportunity to determine organ clearance of substances that are removed from the body by only one organ. Assuming the rate of excretion from the body is directly proportional to the concentration in the plasma, we can determine the instantaneous extraction rate of a particular organ by measuring the rate of change of the substance in the body and the plasma concentration. The volume clearance rate, C_v is

$$C_v(t) = -\left(\frac{dA_t(t)}{dt}\right)/C_p(t) \text{ ml sec}^{-1} \quad . \qquad (2)$$

where $C_p(t)$ is the plasma concentration and A_t is the whole-body activity. The derivative $dA_t(t)/dt$ is an excretion rate from the entire body. Thus, if the relative change in whole-body counts is known, and from this we exclude the contribution from the organ of interest and compartment to which the cleared substance is excreted, we have a simple measure of function. This is an improvement over shielded whole-body counter methods (Oberhausen and Romahn, 1968; Tkocz, H-J. et al., 1971). In the case where multiple organs are involved in the exchange, another analysis applies. The specific activity of any organ exchanging isotope with the blood pool is related to the uptake by all the other organs and the specific uptake or exchange rate of the organ of interest that we designate as K.

For the situation of multiple compartments exchanging with the blood pool, the plasma curve becomes:

$$A(t) = A_1 e^{-\lambda_1 t} + A_2 e^{-\lambda_2 t} \ldots . A_n e^{-\lambda_n t} \qquad (3)$$

If K is the constant exchange rate between a specific organ with activity S, then

$$S = \frac{KA_1}{K-\lambda_1}(e^{-\lambda_1 t} - e^{-Kt}) + \frac{KA_2}{K-\lambda_2}(e^{-\lambda_2 t} - e^{-Kt}) \ldots\ldots + \frac{KA_n}{K-\lambda_n}(e^{-\lambda_n t} - e^{-Kt}). \qquad (4)$$

The exchange rate for a specific organ K_1 can thus be determined by the sequential quantitative whole-body scans by solving Eq. (4) numerically. This parameter extraction project has not reached clinical trials as yet.

THREE-DIMENSIONAL RECONSTRUCTION FROM PROJECTIONS

An advanced goal in nuclear medicine imaging is the quantitative evaluation of the three-dimensional distribution of radionuclide in the body. There are two general categories of imaging techniques applicable to this tractable problem: tomoscanning, which is an imaging technique similar to x-ray laminography or tomography; and digital reconstruction of three-dimensional information from two-dimensional projections or two-dimensional information from one-dimensional projections. The latter category has been variously termed transverse section imaging or scanning, computerized transverse axial tomography, or three-dimensional reconstruction by Fourier or arithmetic methods.

The methods of reconstructing a density distribution from multiple views of an object can be divided into 10 distinct categories, all of which can be shown to be equivalent under special conditions of transformation. The methods are:

1. Matrix inversion direct techniques including generalized inverse or pseudoinverse (Budinger and Gullberg, 1973).

2. Back projection, also known as the summation, superposition, the additive Moire technique, or section scanning (Kuhl and Edwards, 1966; Vainstein, 1971).

3. Iterative least squares technique (ILST)(Goitein, 1972; Budinger and Gullberg, 1973).

4. Algebraic reconstruction iterative technique (ART)(Gordon, Bender and Herman, 1970).

5. Simultaneous iterative reconstruction technique (SIRT)(Gilbert, 1972a).

6. Simultaneous iterative geometric mean technique (Schmidlin, 1972).

7. Back projection of Hilbert transformed projection derivatives (BPHT)(Cormack, 1973; Gilbert, 1972b).

8. High pass filtered back projection (FBP)(Bates and Peters, 1971).

9. Back projection of filtered projections or the convolution technique (BPFP)(Bracewell and Riddle, 1967; Ramachandran and Lakshimininarayanan, 1971; Chesler, 1973; Peters, 1973).

10. Fourier reconstruction technique (FRT)(DeRosier and Klug, 1968; Crowther et al., 1970).

The problem of three-dimensional reconstruction can be simplified by performing a series of two-dimensional reconstructions from multiple one-dimensional projections, then stacking these sections along the rotation axis of the projection views to reconstitute the three-dimensional object (Fig. 5). We have explored most of these techniques, and present here results from the back projection, least squares, and SIRT methods (Fig. 4).

The iterative least squares technique involves the following method for ascertaining the most likely intensity in a particular picture element

$$\Delta A^n(i,j) = A^{n+1}(i,j) - A^n(i,j) = \left[m - \Sigma_\theta \frac{R^n_{k(\theta)}}{P_{k(\theta)}} \right] \Big/ \Sigma_\theta \frac{1}{P_{k(\theta)}} \qquad (5)$$

where n denotes the nth iteration, and m is the number of views. $R_{k(\theta)}$ is the estimated projected density. Equation (5) is the formula involved in finding the set of intensities A(i,j) which will minimize the mean squared error between the estimated projected intensities and the observed projected densities $P_{k(\theta)}$. The subscript $k(\theta)$ denotes the ray passing through the element A(i,j). The reconstruction is controlled from diverging by a damping factor that minimizes the mean squared error between the new estimated projected intensities

$$R^{n+1}_{k\theta} = \sum_{(i,j)\ \epsilon\ \text{ray}\ k\theta} A^n(i,j) + \beta\, \Delta\, A^n(i,j)$$

and the projected intensities. Thus

$$\beta = \frac{\sum_{\theta}\sum_{k}\left[P_{k\theta} - R^{n}_{k\theta}\right]\left(\sum_{(i,j)\,\varepsilon\,\text{ray}\,k(\theta)} \Delta^{n} A(i,j)\right)/P_{k\theta}}{\sum_{\theta}\sum_{k}\dfrac{\left(\sum_{(i,j)\,\varepsilon\,\text{ray}\,k(\theta)} \Delta A_{(i,j)}\right)^{2}}{P_{k\theta}}}$$

The new intensities after each iteration n+1 are

$$A^{n+1}(i,j) = \max\left[A^{n}(i,j) + \beta\,\Delta\,A^{n}(i,j)\,;0\right]$$

Comparison of methods and resolution.

A comparison of the iterative least squares technique to SIRT and to the back projection is shown in Fig. 6 for hot spot detection, and Fig. 7 for void detection. The superiority of 10 ILST iterations to 20 SIRT iterations can be seen in these comparisons. Another criterion of the capabilities of an algorithm is the root-mean-square deviation between the real object and the calculated reconstruction normalized to the deviation of the initial solution.

$$\left|\frac{\sum_{ij}\left(A'(i,j) - A^{n}(i,j)\right)^{2}}{\sum_{ij}\left(A'(i,j) - A^{o}(i,j)\right)^{2}}\right|^{1/2}$$

Using this criterion, the least squares technique was compared to the additive SIRT method at each iteration (Fig. 8).

An example of the results of the ILST technique is shown for a head phantom with lesions 2.5 cm and 4 cm filled with isotope concentration 2 times that of the background (Fig. 3). A total of 1 mCi was used, and 18 conjugate views of 30 sec duration each were taken before a single gamma camera. A patient study is shown in Fig. 9 wherein 18 conjugate views were taken six hours after 8 mCi were injected in a 14-year old girl with a suspected brain lesion. In this case an extended tubular collimator was used to compensate for the distance between the camera and head occasioned by the patient's shoulder.

If a reconstructed image is to be uniformly resolved to a resolution d of a completely unsymmetrical object, the number of discrete views must be at least

$$n \simeq \pi\, D/d$$

where D is the dimension of the object (Crowther et al., 1970; Klug and Crowther, 1972). Thus for a resolution of 1.5 cm in imaging a head 20 cm in diameter, we need 42 views. In practice only 20 views are necessary for the class of objects of importance to nuclear medicine. An explanation for this discrepancy is that 42 projections would be required for an object that has no symmetry, thus no regional correlation.

Of course this is not true for any image, as there is great departure from complete randomness just in the fact that a recognizable image exists. Thus it is not surprising to find the number of views required for reconstructing a two-dimensional distribution with a resolution distance of 1.5 cm far less than the theoretical for images of no symmetry. Another way of understanding the reason for the discrepancy is that in the class of objects of concern many different objects are essentially identical. The resolution, and to a great extent appearance of artifacts, is related to how close the axis of rotation is to a center of symmetry. For example, multiple views of a right cylinder taken around an axis that is displaced from the center of rotation will give a reconstruction that is distorted and contains "clutter" outside the object region (Peters, 1973). Only a single view of the same right cylinder is necessary if the cylinder is in the assumed center of rotation for the reconstruction. However, no *a priori* assumption can be made regarding the topology of a cross section.

Whereas, the iterative least squares technique gives good resolution without artifacts, the BPFT technique has a speed capability that might lead to its preferred use if absorption can be properly handled by this latter method. The ILST and BP methods have been implemented on our small nuclear medicine computer system HP-5407. Clinical trials have just now begun, and early results clearly show these techniques as important advances in quantitative nuclear medicine. Sections of 46 X 46 for 18 conjugate (36) views are calculated in 2 min per iteration by the ILST method using FORTRAN on our small computer (HP-2100A) in the HP-5407 system (Budinger, 1973).

SUMMARY

The whole body scanner can quantitate the regional and sequential distribution of radionuclide on an organ by organ basis using conjugate views and a theoretically valid correction factor if the target to nontarget ratio is high (>4:1). A more precise quantitative technique is the three-dimensional reconstruction of radionuclide distribution from multiple two-dimensional projections. The scintillation camera with an extended collimator is adequate for three-dimensional imaging with 1.5 cm resolution if the patient is rotated in 10° increments and images are obtained with about 15,000 dots per view. Application to brain and myocardial imaging are immediate clinical objectives with important potential. Programs for the full implementation are available from Budinger and Gullberg (1973).

REFERENCES

Anger, H. O. Whole-body scanner Mark II. J. Nucl. Med. 7, 331, 1966.

Bates, R. H. T., Peters, T. M. Towards improvements in tomography. New Zeal. J. Sci. 14, 883-896, 1971.

Bracewell, R. N., Riddle, A. C. Inversion of fan-beam scans in radio astronomy. Astrophys. J. 150, 427-434, 1967.

Budinger, T. F. Clinical and research quantitative nuclear medicine system. In Medical Radioisotope Scintigraphy, vol. 1 (Symp., Monte Carlo, 1972), IAEA, Vienna, 501-555, 1973.

Budinger, T. F., Gullberg, G. T. Three-dimensional reconstruction in nuclear medicine by iterative least squares and free transform techniques. Lawrence Berkeley Laboratory Report No. 2145, 1973.

Chesler, D. A., Hoop, B. Jr., Brownell, G. L. Transverse section imaging of myocardium with $^{13}NH_4$. J. Nucl. Med. 14, 623, 1973.

Cormack, A. M. Reconstruction of densities from their projections, with applications in radiological physics. Phys. Med. Biol. 18, 195-207, 1973.

Crowther, R. A., De Rosier, D. J., Klug, A. The reconstruction of a three-dimensional structure from projections and its application to electron microscopy. Proc. Roy. Soc. Lond. A 317, 319-340, 1970.

De Rosier, D. J., Klug, A. Reconstruction of three dimensional structures from electron micrographs. Nature 217, 130-134, 1968.

Gilbert, P. Iterative methods for the three-dimensional reconstruction of an object from projections. J. Theor. Biol. 36, 105-117, 1972a.

Gilbert, P. F. C. An iterative method for three-dimensional reconstruction from electron micrographs. Proc. Fifth European Cong. Electron. Microsc. 602-604, 1972b.

Goitein, M. Three-dimensional density reconstruction from a series of two-dimensional projections. Nuclear Instruments and Methods 101, 509-518, 1972.

Gordon, R., Bender, R., Herman, G. T. Algebraic reconstruction technique (ART) for three-dimensional electron microscopy and X-ray photography. J. Theor. Biol. 29, 471-481, 1970.

Klug, A., Crowther, R. A. Three-dimensional image reconstruction from the viewpoint of information theory. Nature 238, 435-440, 1972.

Kuhl, D. E., Pitts, F. W., Sanders, T. P., Mishkin, M. M. Transverse section and rectilinear brain scanning with Tc^{99m} pertechnetate. Radiol. 86, 822-829, 1966.

Kuhl, D. E., Edwards, R. Q., Ricci, A. R., Reivich, M. Quantitative section scanning using orthogonal tangent correction. J. Nucl. Med. 14, 196-200, 1973.

Oberhausen, E., Romahn, A. Bestimmung der Nierenclearance durch externe Gamma-Strahlenmessung. In Kreislaufforschung und Kreislaufdiagnostic, 5 (Jahrestagung der Ges. f. Nuclearmedizin, Vienna, 1967), Shattauer Verlag, Stuttgart, 323, 1968.

Peters, T. M., Smith, P. R., Gibson, R. D. Computer aided transverse body-section radiography. Brit. J. Radiol. 46, 314-317, 1973.

Ramachandran, G. N., Lakshminarayanan, A. V. Three-dimensional reconstruction from radiographs and electron micrographs: application of convolutions instead of Fourier transforms. Proc. Nat. Acad. Sci. USA 68, 2236-2240, 1971.

Schmidlin, P. Iterative separation of sections in tomographic scintigrams. Nuclear Med. 11, 1-16, 1972.

Sorenson, J. A. Methods for quantitating radioactivity *in vivo* by external counting measurements. (Ph.D. Thesis), University of Wisconsin, 1971.

Tkocz, H-J., Oberhausen, E., Glöbel, B. Measurement of liver clearance rate with partially shielded whole body counter. In Dynamic Studies with Radioisotopes in Medicine, IAEA, Vienna, 409, 1971.

Vainshtein, B. K. Finding the structure of objects from projections. Soviet Physics--Crystallography 15, 781-787, 1971.

Table 1. Accuracy of calculated activity using eq. 1.

Thickness (cm)	True activity	Calculated activity*	Percent error
^{99m}Tc (Efficiency factor: 3.2×10^{-3})			
2.0	16.0	15.3	-4.4
7.0	16.0	16.1	+0.6
7.0	52.8	54.8	+3.78
10.0	52.8	52.8	0.0
12.5	52.8	51.5	-2.46
^{131}I (Efficiency factor: 7.4×10^{-3})			
10.3	28	27.5	-1.78
10.3	114	110	-3.5
12.4	28	26.6	-5.0
12.4	114	119	+4.38
13.0	36	33.3	-7.5
13.0	81	75.8	-6.41
14.4	28	26.4	-5.7
14.4	114	118	+3.5

*Calculated from efficiency factor X C_t (Fig. 2) X geometric mean.

TABLE 2. Percent of initial activity in body regions.

Area/Time	Day 0	1 (19 hr)	2 (47 hr)	4	6	8	11	13	18	22
Skull	0.2	.22	.14	.07	.05	.04	.04	.02	.02	--
Brain	1.6	.87	.64	.29	.17	.13	.12	.12	.14	--
Face	3.4	2.2	1.3	.72	.42	.34	.32	.30	.22	
Thyroid	0.9	.7	.55	.36	.35	.34	.28	.31	.33	.43
Chest	16.2	8.2	5.6	3.0	2.2	1.4	1.8	1.32	.93	.89
Liver	24.4	12.5	7.1	4.1	2.4	1.4	1.2	1.08	.74	.71
Spleen	3.3	2.5	1.7	.74	.54	.32	.27	.23	--	--
Gut	24.4	26.5	17.7	8.2	6.3	4.7	4.1	3.50	2.59	--
Bladder	1.7	2.8	2.0	0.69	.68	.35	.27	.36	.16	
Arms	7.8	4.5	2.9	1.7	1.3	1.2	1.0	.66	.61	
Legs	15.9	11.5	6.0	4.0	3.0	2.7	1.9	2.2	1.77	--
Gall Bladder		2.2	1.2	.93	.49	.31	.24	.20	.12	

FIGURE CAPTIONS

Fig. 1: Correction factor applied to the results of the geometric mean of supine and prone scans described as a function of thickness of the patient. The factor is not very sensitive to the fraction of the thickness wherein the isotope is distributed.

Fig. 2: Results of a sequential imaging after 3 mCi injection of rubidium-81 (contaminated with 20% rubidium-82*m*) using the Mark II whole-body scanner. The shift from central circulation to liver and peripheral tissues can now be quantitated with an accuracy of less than 10%.

Fig. 3: Anterior and posterior whole-body scans show the sequential distribution of a radiopharmaceutical and allows one to extract quantitative data on the fractional distribution of the dose with respect to regions in the body and time (cf. Table 2).

Fig. 4: There are at least five direct methods that involve reconstruction from multiple views. The techniques compared in this paper are designated by asterisks (*).

Fig. 5: Phantom study demonstrating the ability of least-squares reconstruction technique to delineate the position of two hot spots from 18 conjugate views using the scintillation camera. One mCi was used with a counting period for each view of 15 seconds.

Fig. 6: Comparison of three techniques of three-dimensional reconstruction from 18 views taken at 10° increments on a ring phantom that has two hot spots. Note the ability to distinguish the 1-cm lesion, and the superiority of the least squares and SIRT techniques to the back-projection technique.

Fig. 7: Demonstration of the ability of three-dimensional reconstruction techniques to delineate holes in a liver-phantom slice. The superiority of least squares over other techniques for this bypt of object is demonstrated here.

Fig. 8: A comparison of the SIRT to the least-squares algorithm for two objects. The deviation between the two objects and the reconstructed object is less for the least-squares algorithm than the SIRT algorithm. The least-squares technique takes two minutes per plane on a small computer (HP-2100A).

Fig. 9: Cross-sectional images produced by the ILST after 18 conjugate views of 14 y.o. patient's head 6 hrs after 8 mCi ^{99m}Tc-pertechnetate. Suspected craniopharyngioma.

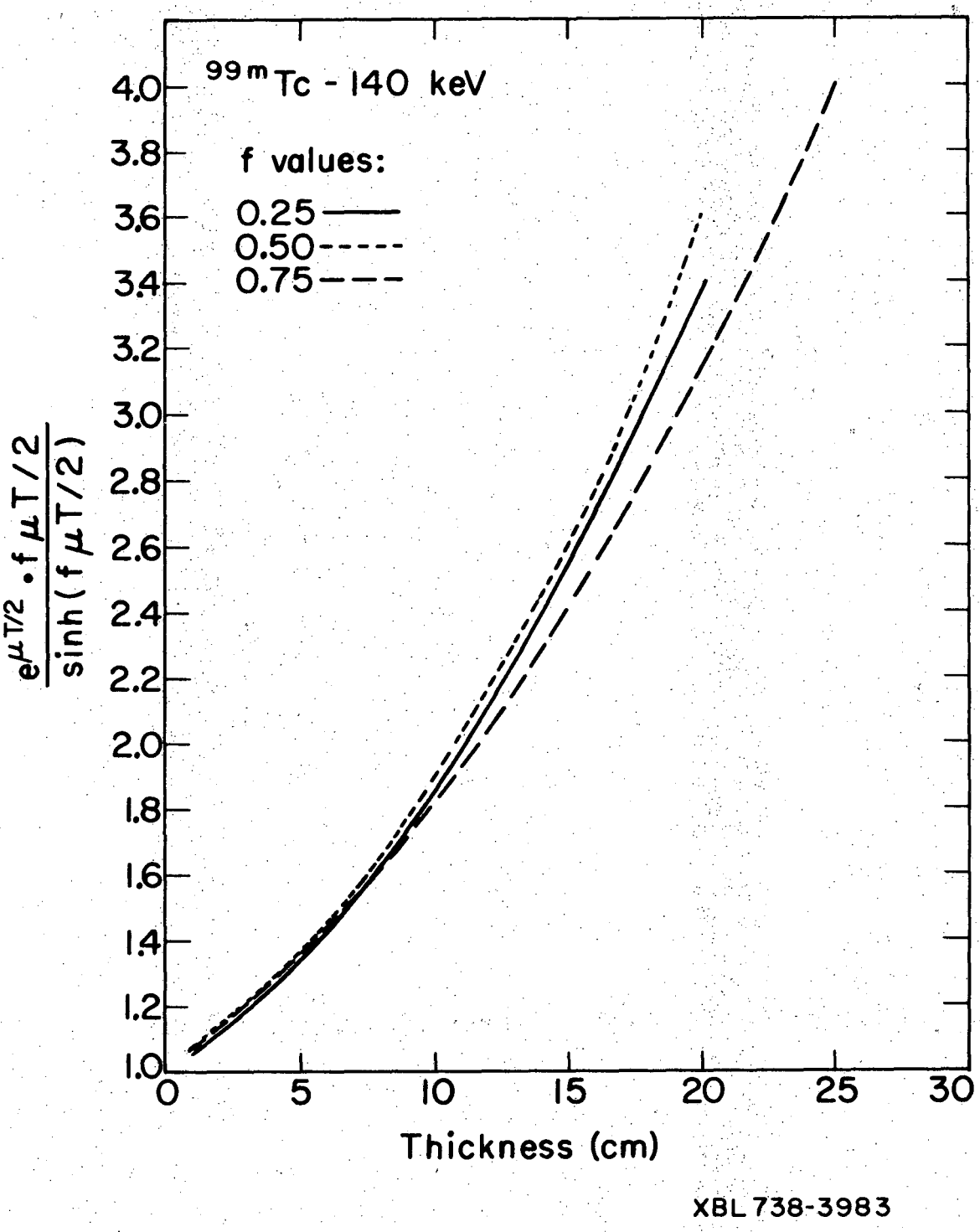
99m Tc - 140 keV
f values:
0.25
0.50
0.75
$\frac{e^{\mu T/2} \cdot f\mu T/2}{\sinh(f\mu T/2)}$
Thickness (cm)
XBL738-3983

Fig. 1

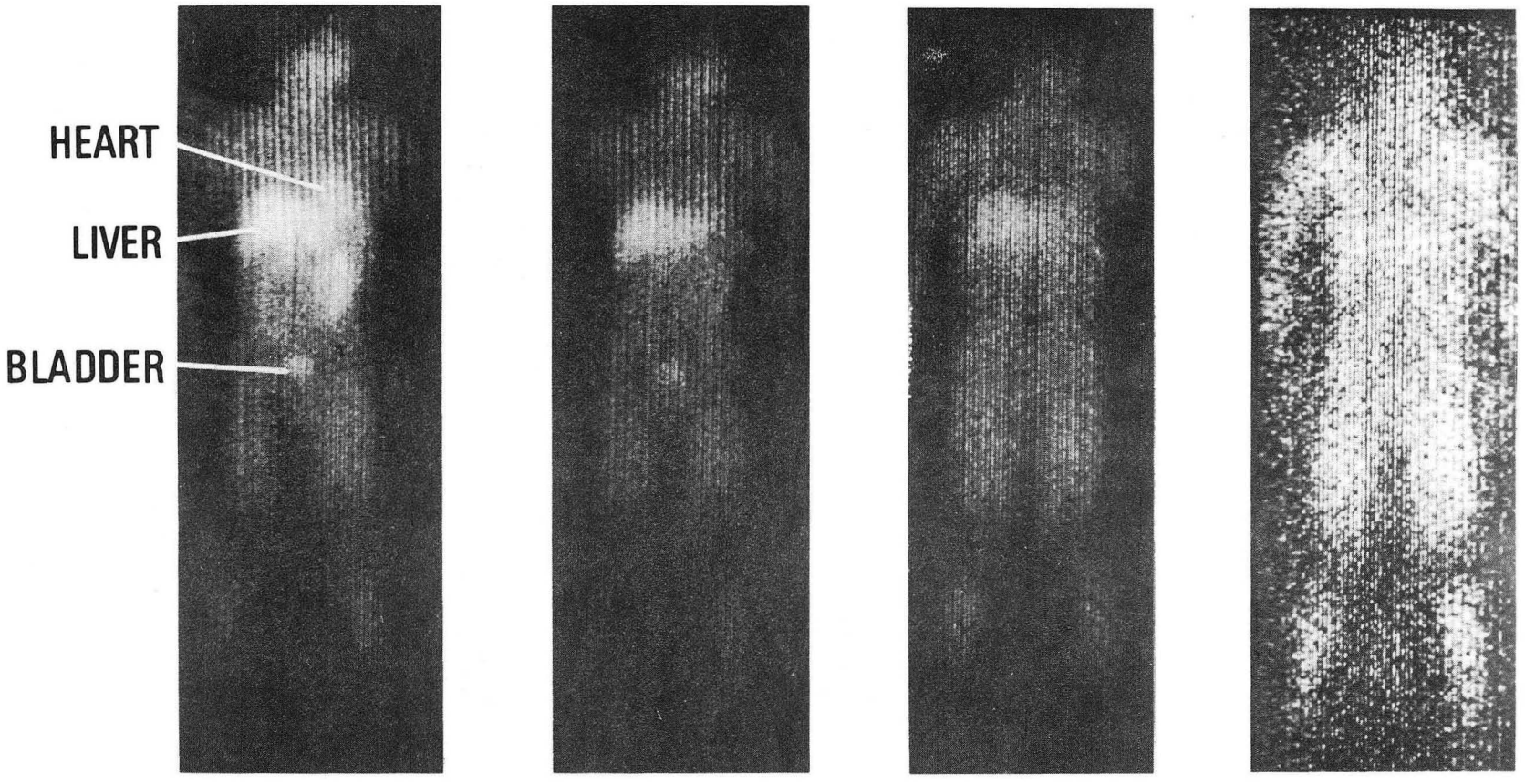
ANTERIOR SCAN WITH RUBIDIUM-81
HEART
LIVER
BLADDER
1
4
22
44
Hours after 3 mCi i.v.
XBB 735-1226

Fig. 2

SERIAL WHOLE BODY SCANS SHOWING DISTRIBUTION OF ^{131}I-19-IODOCHOLESTEROL

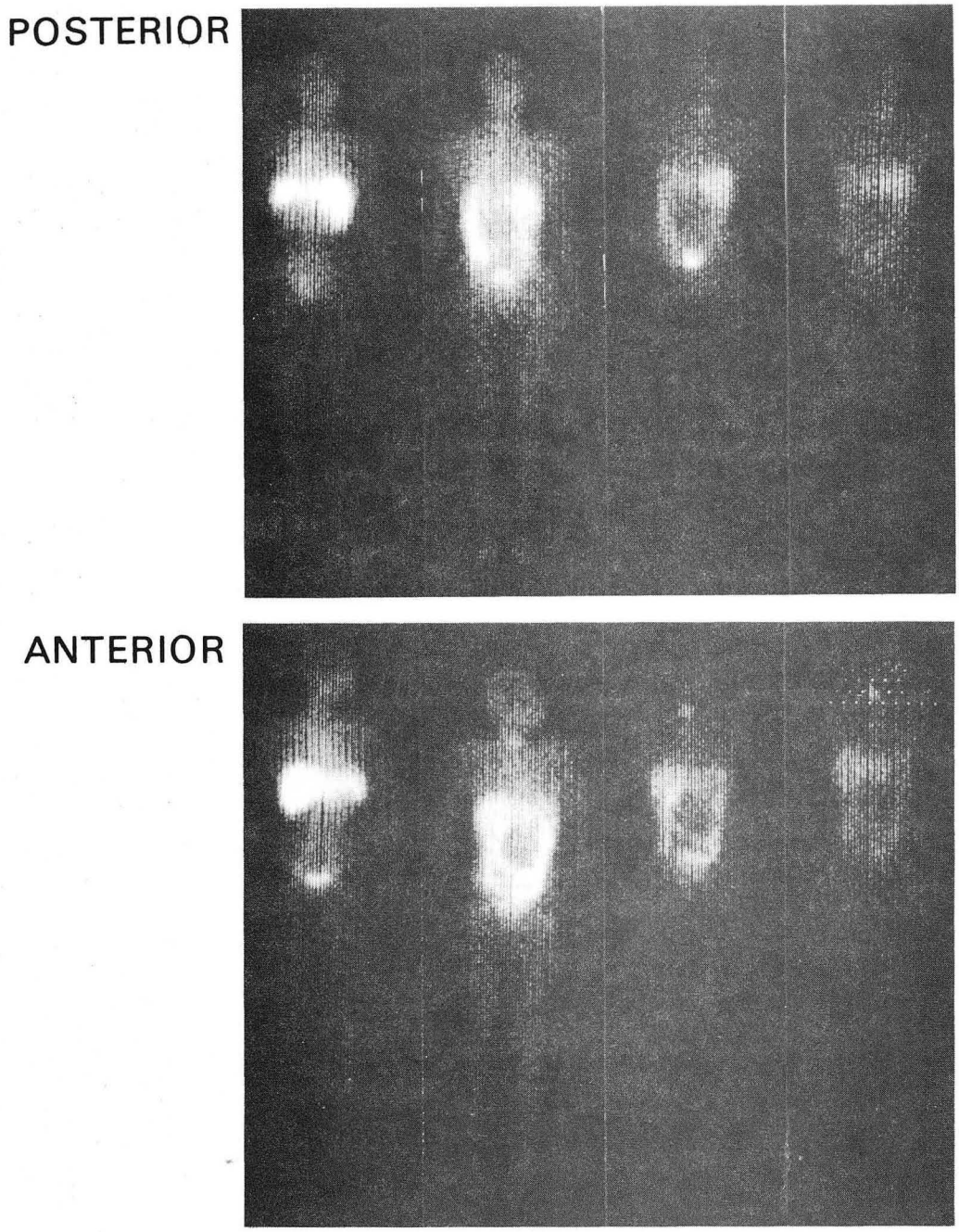

Fig. 3

Direct methods

Matrix inversion

* Back projection

Hilbert transform $\left\{\frac{dP_{k(\theta)}}{dk}\right\}$ then back project

A.R.T.

* S.I.R.T.

* Least squares

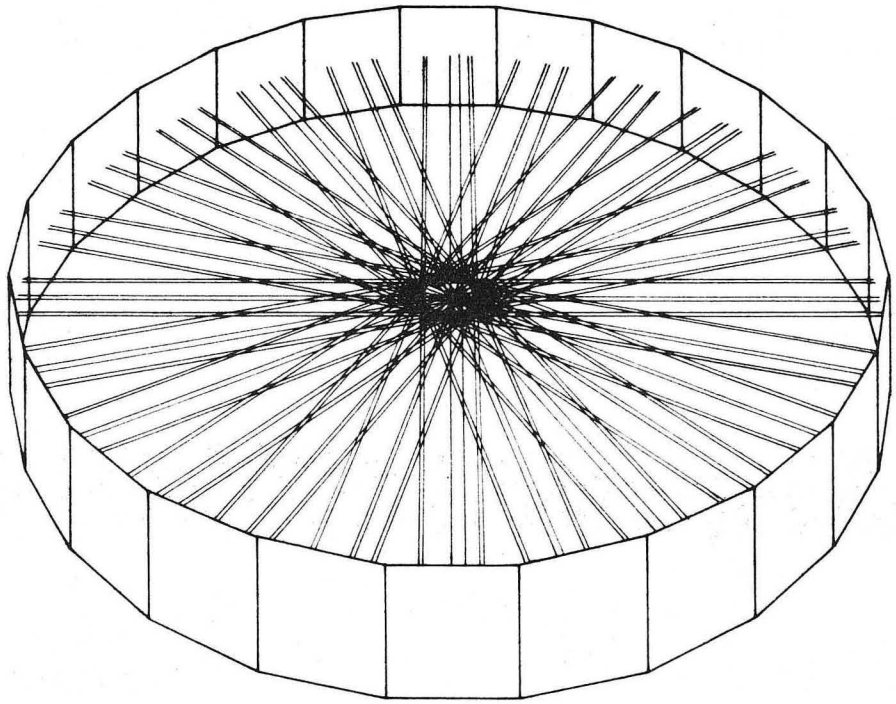

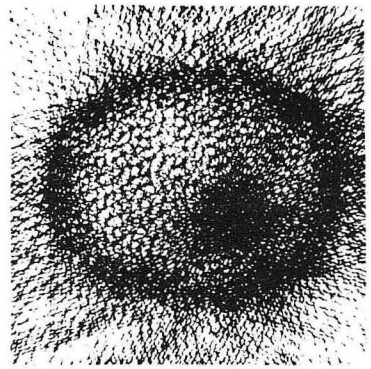

XBL737-3616

Fig. 4

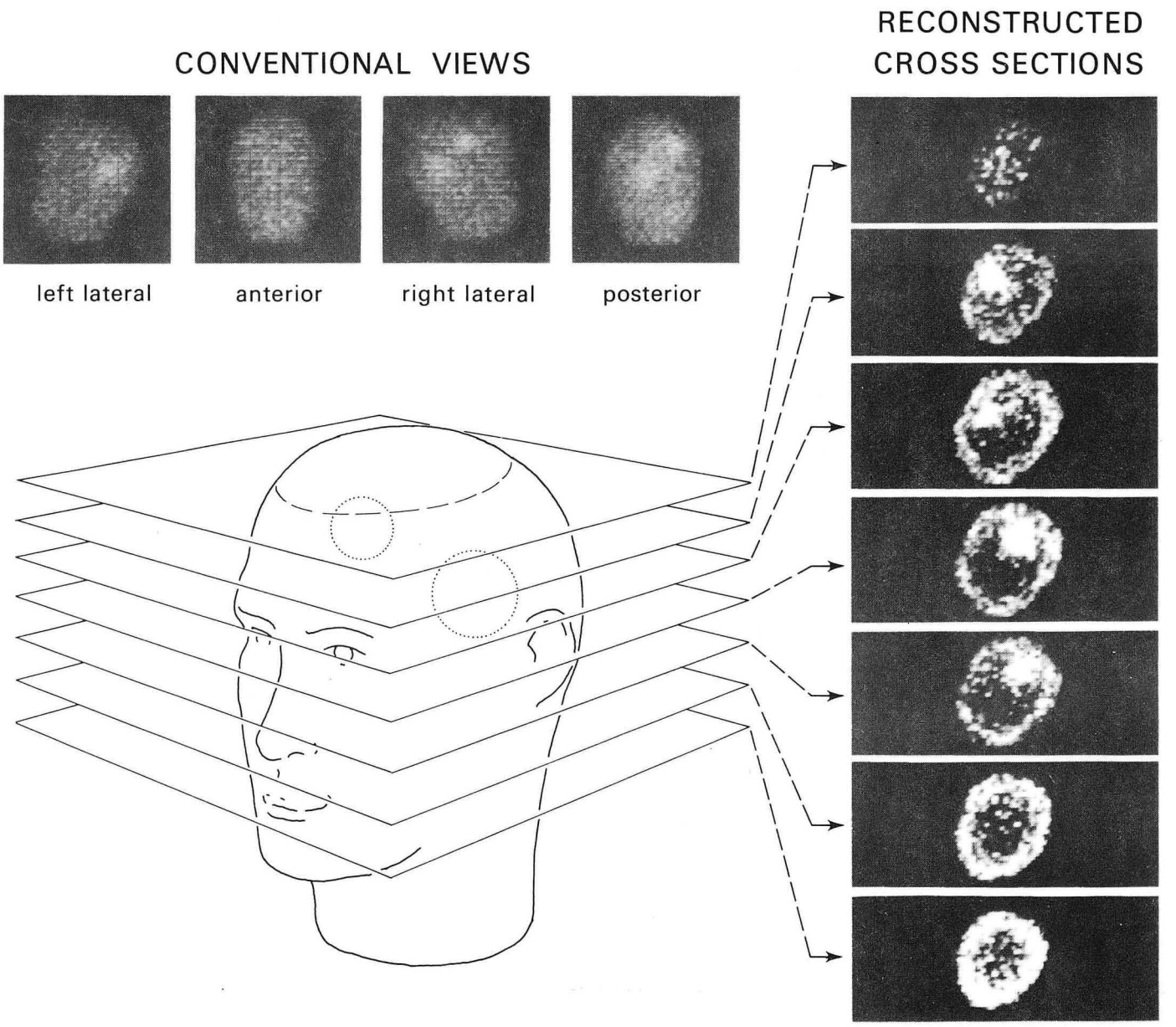

XBB 737-4161

Fig. 5

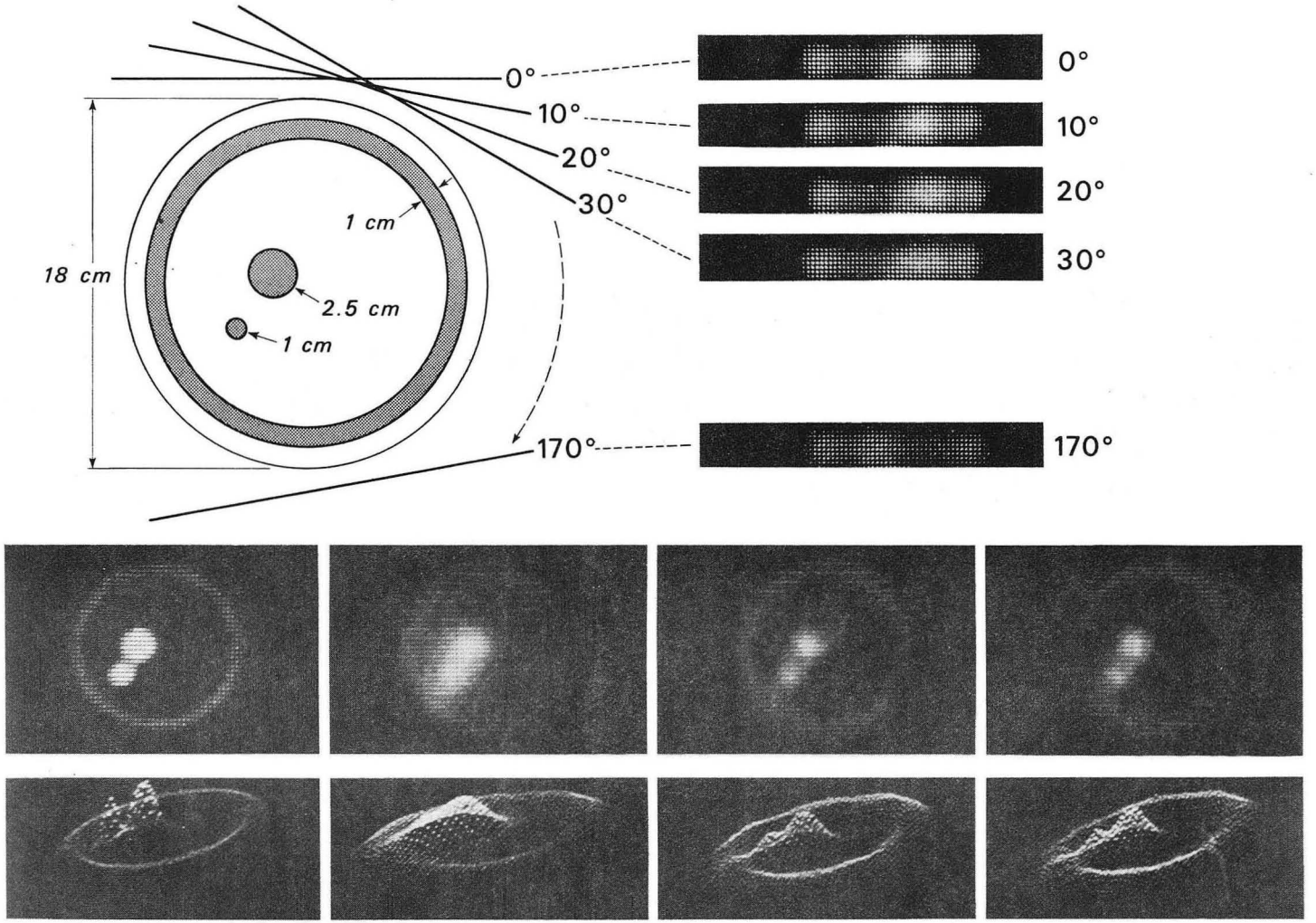

XBB 736-4065

Fig. 6

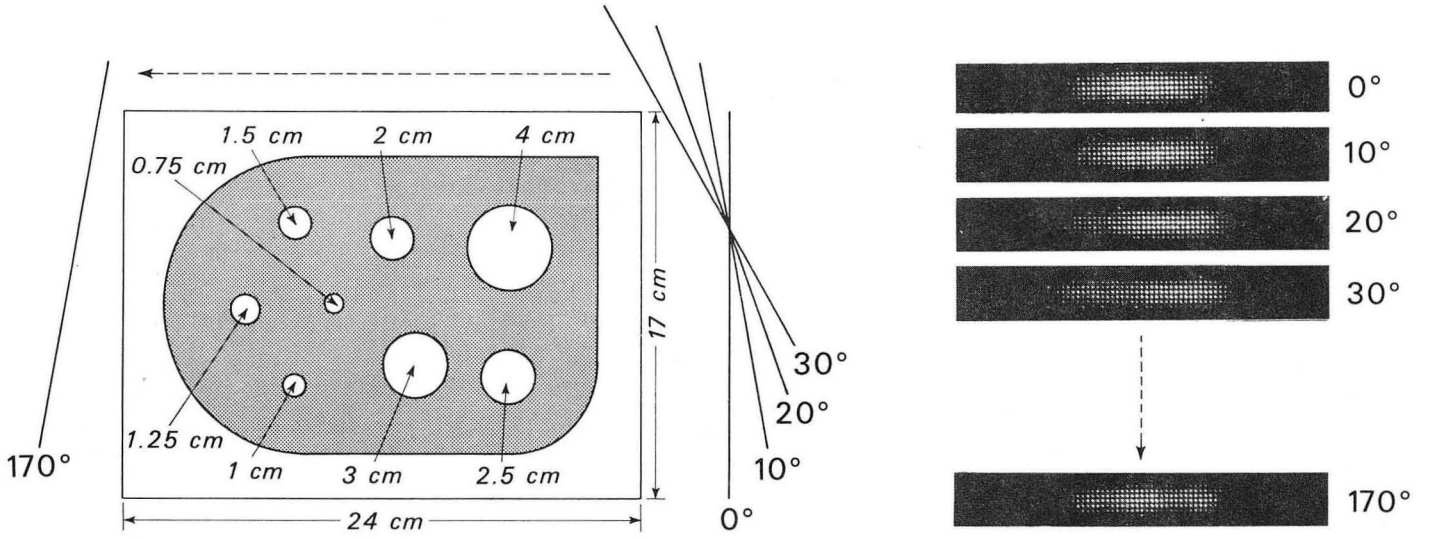

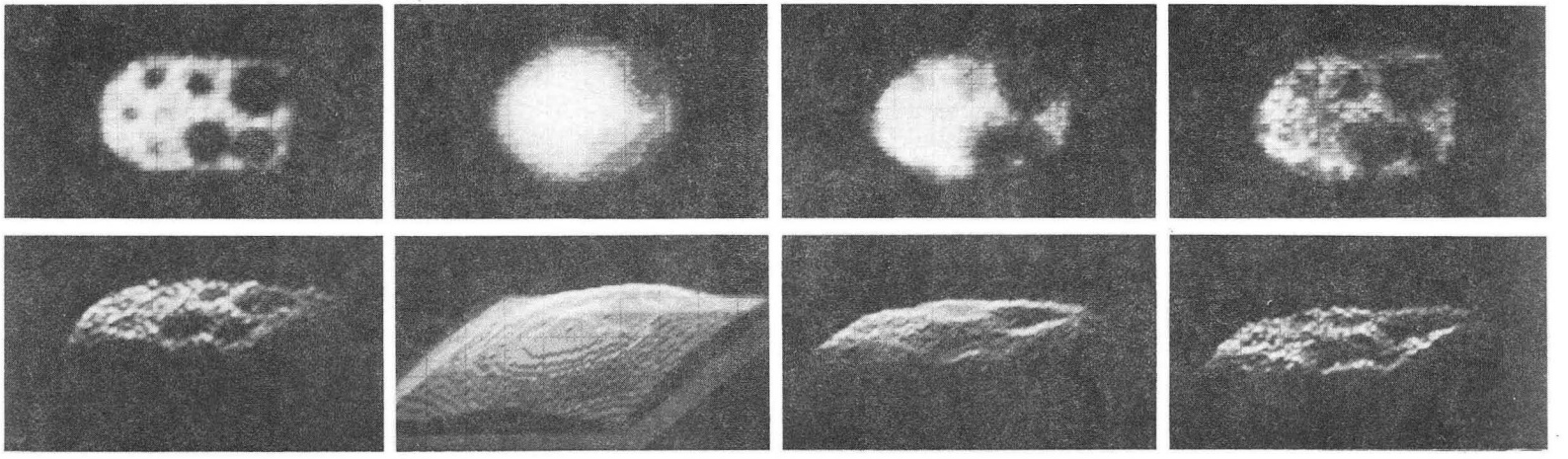

XBB 736-4066

Fig. 7

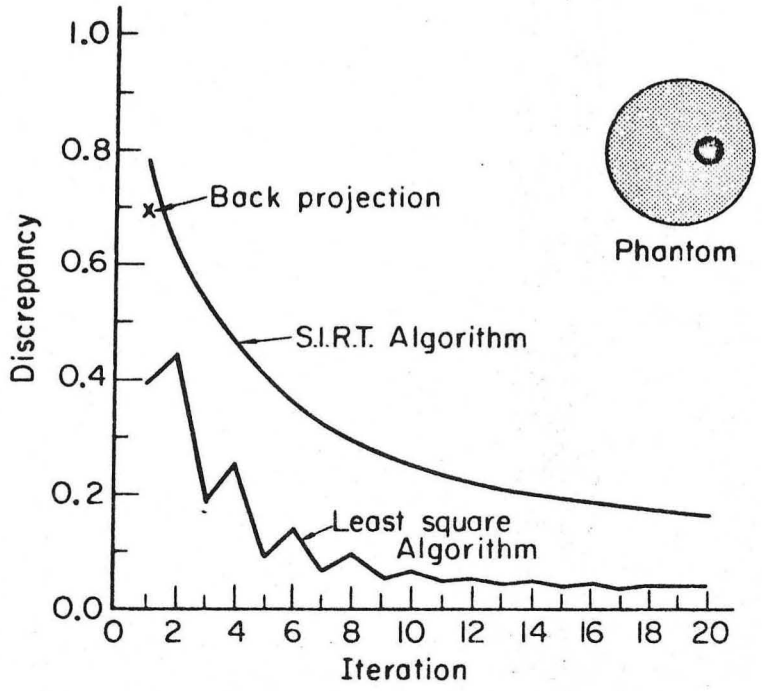

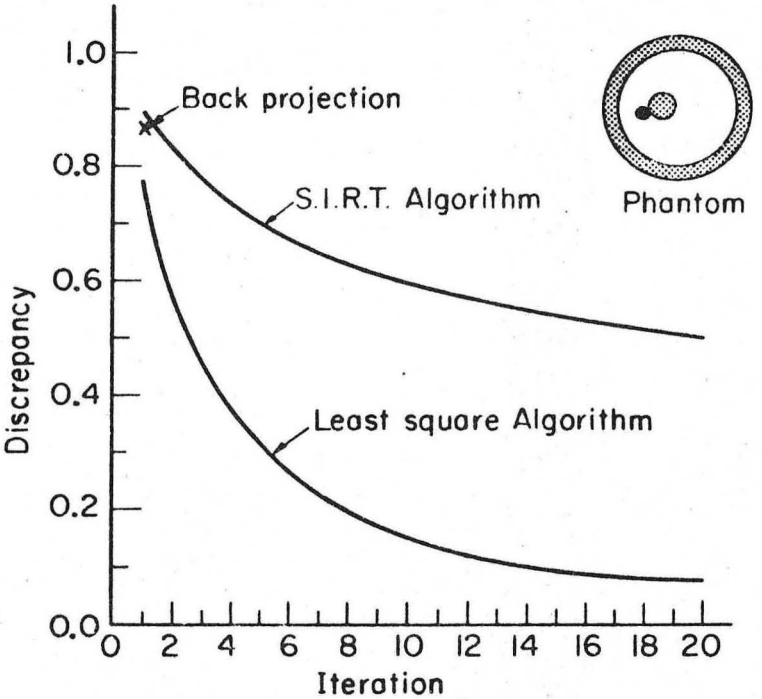

$$\text{Discrepancy} = \left[\sum_{i,j} (\rho'_{ij} - \rho^n_{ij})^2\right]^{1/2} \Big/ \left[\sum_{i,j} (\rho'_{ij} - \rho_{oij})^2\right]^{1/2}$$

XBL 738-3864

Fig. 8

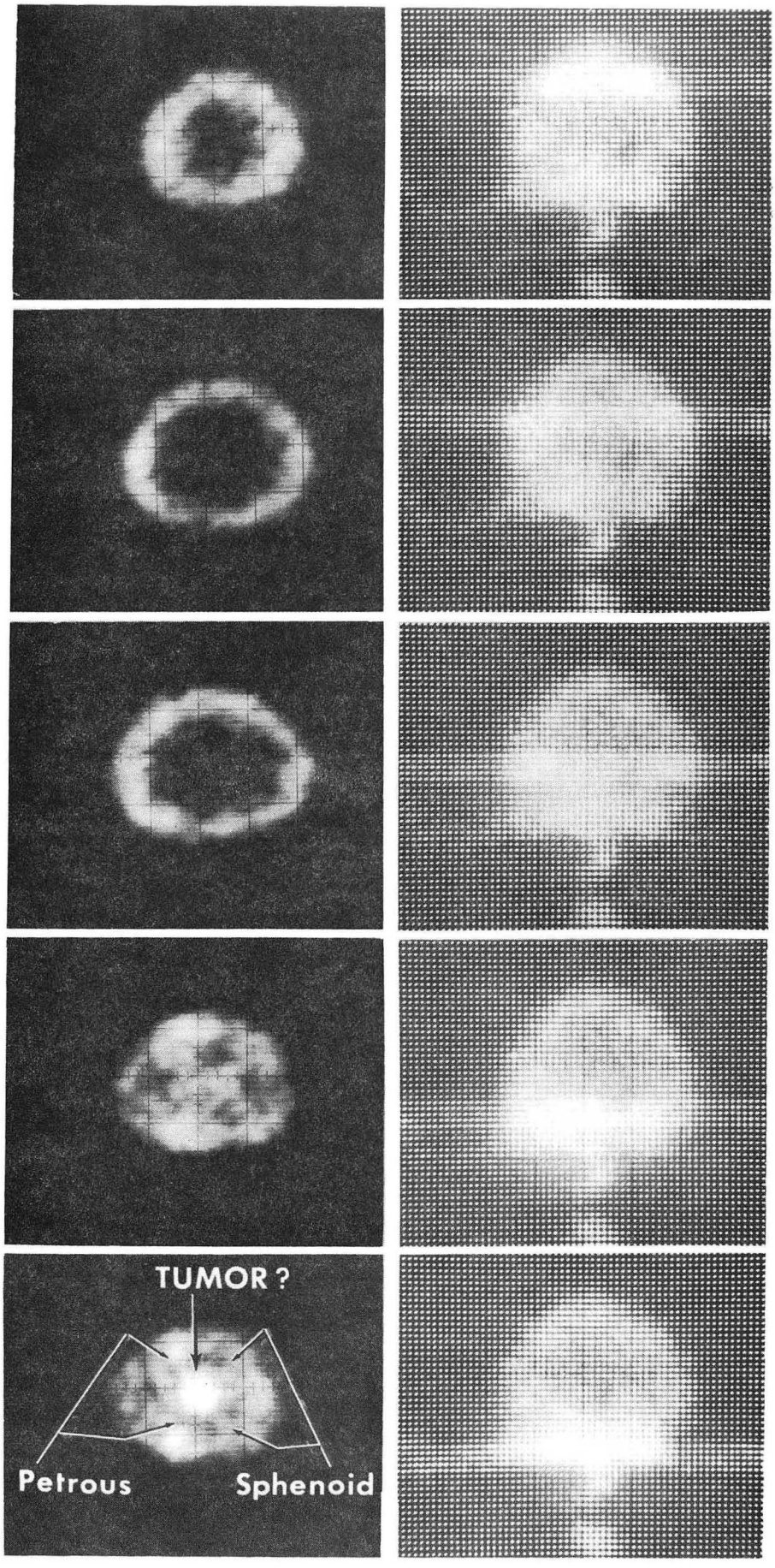

XBB 739-5135

Fig. 9

TECHNICAL INFORMATION DIVISION
LAWRENCE BERKELEY LABORATORY
UNIVERSITY OF CALIFORNIA
BERKELEY, CALIFORNIA 94720